



Numerical measurement of flow fluctuations to quantify cohesion in granular materialsNicolas Preud'homme *, Geoffroy Lumay, Nicolas Vandewalle, and Eric Opsomer
GRASP, University of Liège, B-4000 Liège, Belgium (Received 20 May 2021; revised 11 October 2021; accepted 18 November 2021; published 15 December 2021)

The flow of cohesive granular materials in a two-dimensional rotating drum is investigated using discrete element method simulations. Contacts between particles are modeled based on the widely used model of the spring-dashpot and Coulomb's friction law. A simplified model of intermediate range attraction between grains (i.e., cohesion) has been used in order to reproduce the flow of electrostatic or wet granular materials. Granular flow is generated by means of a rotating drum and the effect of the rotation speed, the friction between the grains, and the cohesion are studied. Significantly different flow behaviors are observed when cohesion is added. Plug flow appears in the rotating drum for a wide range of rotation speeds when cohesion becomes sufficiently strong. We propose a measurement of surface flow fluctuations to quantify the strength of cohesion, inspired by the previous observation of plug flow. Then, we make use of the results to include the effect of cohesion into a theoretical flow model. A good agreement is obtained between theory and numerical measurements of the granular bed's dynamic angle of repose, which allows us to propose a method for estimating the microscopic cohesion between grains based on the measurement of surface fluctuations.

DOI: [10.1103/PhysRevE.104.064901](https://doi.org/10.1103/PhysRevE.104.064901)**I. INTRODUCTION**

Many processes in the pharmaceutical, food, and manufacturing industries involve granular materials handling [1–4]. Among the large amount of industrial processes with granular materials, one finds, for instance, the mixing or separation of different powders as well as pouring or spreading of granular materials. Up to now, these processes have been investigated independently to provide rather specific answers on how they could be affected by the parameters of the granular materials, such as the shape of the grains or the interactions between individual grains. Yet most of these manipulations with granular materials entail a common phenomenon: the flow of granular materials.

Understanding the granular materials' flow often requires the use of a specific experimental setup able to produce a planar shear, an annular shear, a vertical chute, or a heap flow, or setups such as an inclined plane or a rotating drum, which are all reviewed in Ref. [5]. Rotating drums are often considered as the best way to produce a steady granular flow under low confinement pressure [4] due to the fact that they are closed systems with controllable granular flow and a free interface. Investigating granular dynamics in a rotating drum often consists in the measurements of mixing or segregation [6,7], dynamic angle of repose or interface fluctuations [4], or the determination of the velocity profile in the bulk [5,8]. However, the latter task remains challenging and has motivated the development of sophisticated techniques such as the particle tracking method [9], observation with a fast camera [10], positron emission [11,12], and multiple radioactive [13] particle tracking and magnetic resonance imaging [14,15]. More recently, numerical techniques have been employed in

order to avoid the difficulties of implementation and the limitations of experimental techniques.

The experimental and numerical studies show that several regimes of granular flow exist [16,17]. In the case of ideal granular materials where grains interact only by steric contacts, the flow regimes have been extensively studied by Mellmann *et al.* [16], whose summarizing table is reproduced and adapted in Table I. In Table I, one can see that the flow regime primarily depends on the Froude number (Fr), which is a dimensionless number defined as the ratio between inertia and gravity,

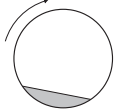
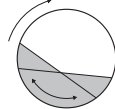
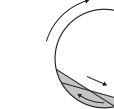

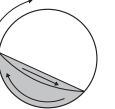
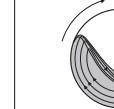
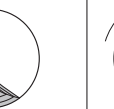
$$\text{Fr} = \frac{\omega^2 R}{g}, \quad (1)$$

where ω is the rotation speed of the drum, R its radius, and $g = 9.81 \text{ ms}^{-2}$. The Froude number is thus directly related to the rotation speed of the drum. The flow regimes also depend on the filling fraction, which is the ratio between the space occupied by the granular bed and the maximum space available inside the rotating drum. When considering more realistic granular materials, one observes differences in this classification and in the measurements of the velocity profile or the dynamic angle of repose. That is how the effect of grain size [4,18], grain shape [19–22], cohesion between grains [23–27], or the boundaries of the drum [15,28,29] have been highlighted.

While grain size, grain shape, and the range of boundary effect can be rather easily quantified, the strength of cohesion between grains requires more sophisticated techniques. In some experimental studies, cohesion is triggered through the variation of relative humidity in the air [23,30] or external magnetic fields are used to induce attractive forces between ferromagnetic grains [31]. However, the direct measurement of the strength of cohesion between grains in cohesive granular materials such as metallic, pharmaceutical, or food powders

*Corresponding author: n.preudhomme@uliege.be

TABLE I. Different possible regimes of granular flow in the rotating drum depending on the filling degree and the rotation speed of the drum given by the Froude number $Fr = \frac{\omega^2 R}{g}$, with ω the rotation speed in rad/s, R the drum radius, and g the gravity. A steady granular flow is obtained only in the rolling and the cascading regimes. Therefore, we performed all of our measurements with rotation speeds of the drum lying within the limits imposed by these regimes. Table adapted from [16].

Regime	Sliding	Surging	Slumping	Rolling	Cascading	Catacting	Centrifuging
Schematic							
Froude number (Fr)	$0 < Fr < 10^{-4}$		$10^{-5} < Fr < 10^{-3}$	$10^{-4} < Fr < 10^{-2}$	$10^{-3} < Fr < 10^{-1}$	$0.1 < Fr < 1$	$Fr \geq 1$
Filling degree	$f < 0.1$	$f > 0.1$	$f < 0.1$	$f > 0.1$		$f > 0.2$	

can hardly be achieved. Still, these types of granular materials are encountered in many applications.

A way to circumvent this difficulty consists in reproducing this particular type of granular flow using numerical simulations and modeling [26,32]. By performing the measurements described above, one observes that cohesion strongly influences granular flow and creates avalanching in the steady flow cascading regime [23]. What is called avalanching is the intermittent flow that appears with cohesion in granular materials. It is characterized by the apparition of grain aggregates that periodically slide at the surface of the granular bed. These aggregates look like avalanches and produce fluctuations in the height of the granular bed's surface.

In the present paper, a method to measure the granular bed surface fluctuations is proposed and related to the strength of cohesion in the granular material. This study is based on two-dimensional (2D) numerical simulations of granular flow in a rotating drum. In 3D rotating drums, end walls have an effect on the flow of granular materials [15,33,34], but it has been shown that this effect was limited to the vicinity of the end walls and could be even further reduced by using smooth end walls [35]. Many experiments or numerical simulations are thus performed in 2D or quasi-2D rotating drums [8,36,37]. First, we describe our numerical model and the implementation of the cohesive interactions between particles. We show that a simplified model for cohesion between grains could be used for such numerical simulations. In the following section, we investigate the effect of the rotation speed, the coefficient of friction between grains, and, most importantly, cohesion. Finally, based on the measurement of surface fluctuations, we adapt the theoretical model of granular flow by Dury *et al.* [15] to take cohesion into account.

II. NUMERICAL MODEL

In order to reproduce granular flow inside a rotating drum, an in-house algorithm based on the soft-sphere discrete element method (DEM) has been developed.

Normal contact forces are modeled using a linear spring dashpot. Each time two grains overlap, a springlike force is applied on each grain involved in the collision. As collisions between grains are inelastic, dissipation is also taken into account by this model via a viscous damper. If two grains come into contact, the expression of the repulsive force on

each grain is given by

$$\mathbf{F}_N = -k_N \delta \hat{\mathbf{n}} - \eta v_N \hat{\mathbf{n}}, \quad (2)$$

where k_N is the spring stiffness, δ is the surface to surface distance between grains, $\hat{\mathbf{n}}$ is the unitary vector pointing from one grain to another, v_N is the normal component of the relative speed at the point of contact, and η is the viscosity given by $\eta = -2 \ln \epsilon \sqrt{mk_N / (\ln^2 \epsilon + \pi^2)}$, with ϵ the coefficient of restitution and m the effective mass of the grains involved in the collision [38,39]. The value of the spring stiffness has been fixed to tolerate a maximum overlap of $r/100$, with r being the grain radius. The same force is used for the contacts between the grains and the drum.

Friction has been implemented in a similar way. Once two grains are in contact and slide onto one another during one time step dt with a relative tangential velocity v_T , a tangential springlike force is added on both grains to mimic static friction. As the spring stretches, this force can increase up to a saturation value which corresponds to the dynamic friction regime. The tangential friction force acting on sliding grains is thus

$$\mathbf{F}_T = \begin{cases} -k_T \delta_T \hat{\mathbf{t}} & \text{if } k_T \delta_T < \mu F_N \\ -\mu F_N \hat{\mathbf{t}} & \text{else,} \end{cases} \quad (3)$$

where $k_T = 2k_N/7$ is the tangential spring stiffness, μ is the coefficient of friction, $\hat{\mathbf{t}}$ is the unitary vector tangential to the surface of the grains and directed in the opposite direction from the tangential velocity v_T , and δ_T is the tangential displacement between the grains defined as

$$\delta_T = \int_t^{t'} v_T dt, \quad (4)$$

where we have $t' = t + dt$. The same force is applied on grains sliding on the drum.

Finally, we introduce intermediate range attraction to reproduce cohesion. In order to facilitate control over the strength and range of such interactions, we propose a model which considers a maximum attraction at contact that decreases quadratically with δ . Curvature is chosen so that the attractive force vanishes at a fixed range corresponding to the radius of a grain, i.e., when $\delta = r$. The intensity of this attraction force is expressed via the Bond number denoted Bo . This dimensionless number is defined as the ratio between the

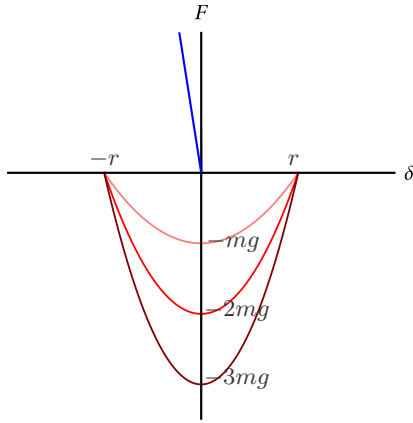


FIG. 1. Force-displacement model used in the simulations, where F is the normal force acting on a grain as a function of the interdistance δ to another grain. The linear repulsion is represented in blue and multiple attraction intensities are represented by the color-graded red curves: light red for $Bo = 1$, red for $Bo = 2$, and dark red for $Bo = 3$.

attractive force at contact F_0 and the weight of the grains,

$$Bo = \frac{F_0}{mg}. \tag{5}$$

We thus define the attractive force between grains as follows:

$$\mathbf{F}_c = F_0 \left[\left(\frac{\delta}{r} \right)^2 - 1 \right] \hat{\mathbf{n}}. \tag{6}$$

On one hand, we have the maximum intensity of cohesion, which is given by $F_0 = mgBo$. The cohesive force is thus a multiple of the weight of the grains. On the other hand, we have the expression $(\delta/r)^2 - 1$, which gives the desired parabolic potential with a maximum range of one grain radius r . To sum up, the force-displacement model chosen is shown in Fig. 1. In addition to the interactions between grains or between grains and the drum, all grains undergo weight with terrestrial gravity.

At each time step, the sum of all forces acting on each grain is calculated. Newton’s equations of motion are then solved numerically using a leapfrog integrator [38]. The main parameters are the speed of rotation of the drum ω , the coefficient of friction μ , and, most importantly, the Bond number Bo . The range of variation for the rotating speed has been chosen so that $20 < \omega < 100$ rpm. The Bond number has a maximum value of 4 in order to avoid creating large bodies of grains rolling in the rotating drum. The coefficient of friction is varied between 0.2 and 1. The fixed parameters are drum radius $R = 0.05$ m, slightly polydisperse grains $0.001 < r < 0.0011$ m with a mass $m = 4 \times 10^{-6}$ kg, coefficient of restitution $\epsilon = 0.9$, and normal spring stiffness $k_N = 200$ N/m. For every simulation, the drum has been filled with 1000 grains to have a drum filling fraction of approximately 50%. Their movement inside the drum has been reproduced during 10 seconds for each set of parameters and data is collected at 20 frames per second. The simulations were run either on a Linux Intel Core i7 computer or on the general computing server Linux Intel X86-64bit from the Service Général d’Informatique (SEGI), University of Liège. Some snapshots

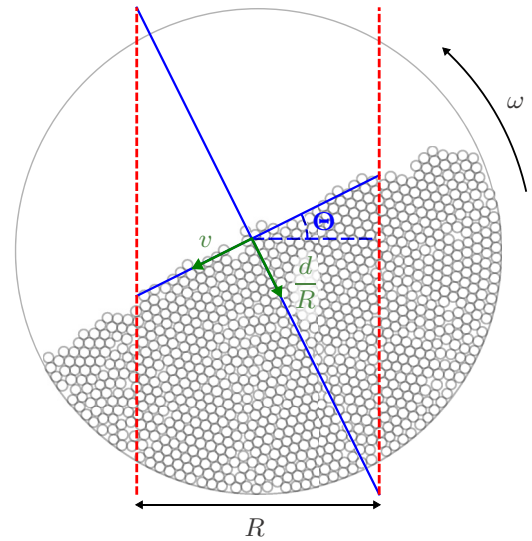


FIG. 2. Reference frame for the measurement of the dynamic angle of repose Θ and the velocity profile $v(d/R)$ (radius R and rotating speed ω). The measurements are performed on the central part of the flow surface delimited by the red dashed lines.

of the resulting granular flow are shown in Table II. We can directly see the influence of the cohesion and the rotation speed on the surface of the flowing granular material. That is the reason why, in the following section, measurements are exclusively performed on the surface of the granular bed.

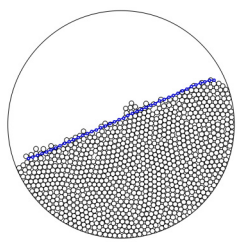
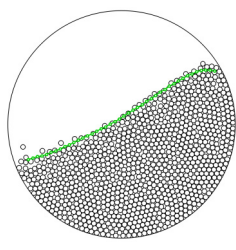
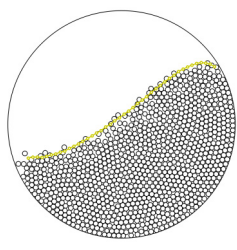
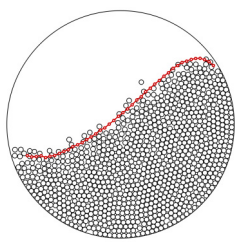
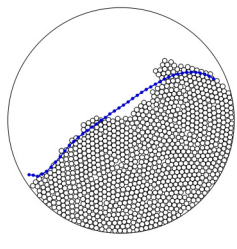
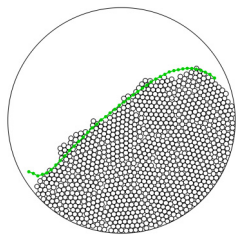
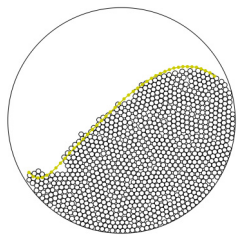
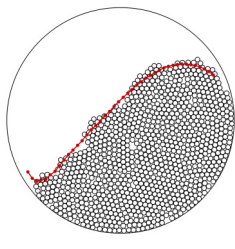
III. GRANULAR FLOW MEASUREMENTS

In the case of noncohesive granular materials, the most frequent measurements carried out are the measurements of the dynamic angle of repose [1,4,15,35] and the velocity profile [10,12,14,40,41]. These measurements were also performed in our study, but required an adaptation to remain relevant in the case of cohesive granular materials. Indeed, as shown in Refs. [25,26], depending on the strength of cohesion between grains and the rotation speed of the drum, the shape of the grain-air interface might become convex. For this reason, the linear fit of the surface flow required for the following measurements should be performed on a limited region of the surface, as suggested by [26]. For our study, we selected the central part of the granular bed to determine the mean surface, as shown in Fig. 2. Each simulation with a set of parameters was reproduced 10 times to avoid statistical errors and more accurately highlights the influence of each parameter on granular flow.

A. Velocity profiles

The velocity profile gives the average speed of the grains as a function of the depth d in the granular bed, as shown in Fig. 2. It is calculated in the rotating reference frame of the drum by subtracting the linear speed of the drum at position d . If we first compare our results with experimental velocity profiles, we observe that the noncohesive curve in Fig. 3(a) is very similar to those obtained experimentally [5,10,40]. Indeed, the characteristic linear decrease of velocity in the

TABLE II. Snapshots of the numerical simulations obtained with the algorithm described in Sec. II. Colored curves indicate the mean surface of the granular bed during the whole simulation, with a color code corresponding to the rotation speed of the drum: blue for 10 rpm, green for 30 rpm, yellow for 50 rpm, and red for 70 rpm. Results are obtained at $Bo = 0$ (noncohesive granular material, represented by empty symbols for the mean surfaces) or $Bo = 2$ (cohesive granular material, represented by filled symbols for the mean surfaces) at different rotation speeds of the drum ω .

ω (rpm) \ Bo	10	30	50	70
0				
2				

flowing layer followed by the exponential decrease in the solid central region is also obtained with our model for noncohesive granular materials. We notice in this same figure that when the cohesion between grains increases, the velocity profiles tend to flatten and stretch. That tendency to flatten at higher Bo is also observed in the numerical simulations of Brewster *et al.* [26] and is due to a well-known distinctive feature of cohesive granular materials: plug flow. As the cohesion increases, the nearly flat velocity profile appearing at the surface of the granular bed (e.g., at $d/R \sim 0$) means that the grains begin to flow with the same velocity. Some larger clusters of grains are thus sliding on the granular bed. This effect is called plug flow. We also notice that the velocity profiles stretch when the cohesion increases, which means that the surface of the granular flow is rising. When Bo increases, the surface changes from a concave S shape to a convex shape, which explains this elevation of the surface interpreted from the velocity profiles. This effect of the cohesion was also expected as it is the reason why we adapted the measurement techniques as explained above.

The effect of the rotation speed on the flow of cohesive granular materials is shown in Fig. 3(b). We first observe that a constant velocity profile seems to develop at the surface of the granular bed when the rotation speed is increased. As classified by Mellmann [16], the granular flow for large rotation speeds is in the centrifuging regime. For the largest values of ω chosen here, we are at the limit of this regime and hence the grains might begin to fly away from the surface in a parabolic motion. With the action of cohesion, larger clusters are formed and flow down. We can thus assume that plug flow is enhanced by large rotation speeds in cohesive granular materials.

Second, we notice that when the rotation speed becomes relatively large, the grains in contact with the drum (e.g., at

$d/R = 1$) move slightly slower than the drum itself because the grains have a velocity relative to the drum which is not equal to zero at this position. This tells us that grains are sliding on the drum. Once the rotation speed is too large, the granular bed is no longer able to follow the drum rotating beneath it.

Increasing the coefficient of friction allows the grains to stick to the drum, as shown in Fig. 3(c). On this graph, we actually notice that when μ is large, the grains at contact with the drum and the drum move at the same velocity. The straight line obtained at $\mu = 0.2$ tells us that all the grains of the granular bed are sliding and thus motionless in the laboratory reference frame. Indeed, as the velocity is measured in the reference frame of the drum, when the drum rotates and all the grains stay at their position, the velocity profile obtained is actually given by ωd .

B. Dynamic angle of repose

The dynamic angle of repose Θ is easily obtained with the fit of the mean surface, as shown in Fig. 2. The effects of the three main parameters have been investigated and the results are shown in Figs. 4(a)–4(c). Ignoring momentarily the dashed curve obtained with the theoretical model which will be presented in Sec. III D, we first notice in Fig. 4(a) that the dynamic angle of repose for a noncohesive granular material evolves linearly with the rotation speed with a change of slope at around 50 rpm. These results are similar to the experimental results reported by [15,35], which identified the change of slope as a transition to the S-shaped surface. The value of 50 rpm that we obtain with our system also corresponds to the critical Froude value for the transition from the rolling regime to the cascading regime calculated by Mellmann [16].

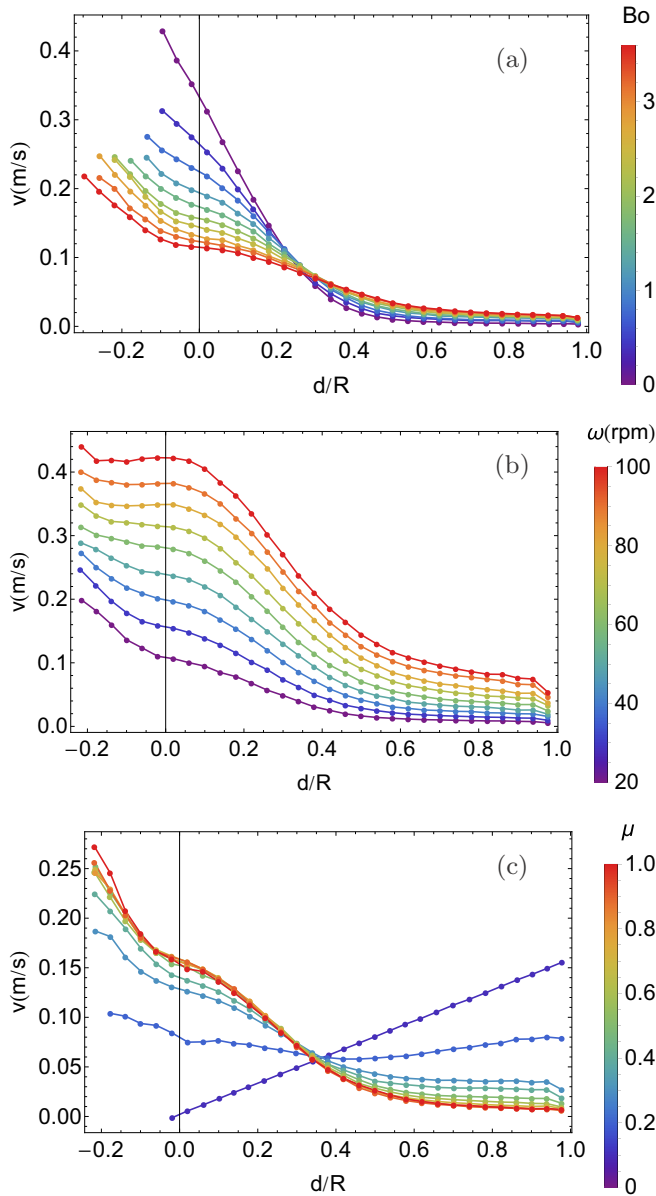


FIG. 3. Numerical measurement of the velocity profiles for different values of the parameters studied. (a) Influence of cohesion at $\omega = 30$ rpm and $\mu = 0.6$, (b) influence of the rotation speed of the drum at $Bo = 2$ and $\mu = 0.6$, and (c) influence of the coefficient of friction at $Bo = 2$ and $\omega = 30$ rpm.

A constant linear increase is observed when cohesion is added and the change of slope disappears, which shows that the transition to the S-shaped regime does not occur at the same rotation speed when there is cohesion between grains.

The effect of the cohesion is shown in Fig. 4(b). We observe that as Bo increases, the dynamic angle of repose starts to saturate. This tendency was also observed in the numerical simulations of Brewster [26] and interpreted as a competition between the speed of rotation of the drum and the cohesion between the grains. Due to cohesion, the surface changes from a linear shape or S shape, if the rotation speed is high enough, to a convex shape. Once the cohesion is too high, the attractive forces completely overcome inertia and the surface

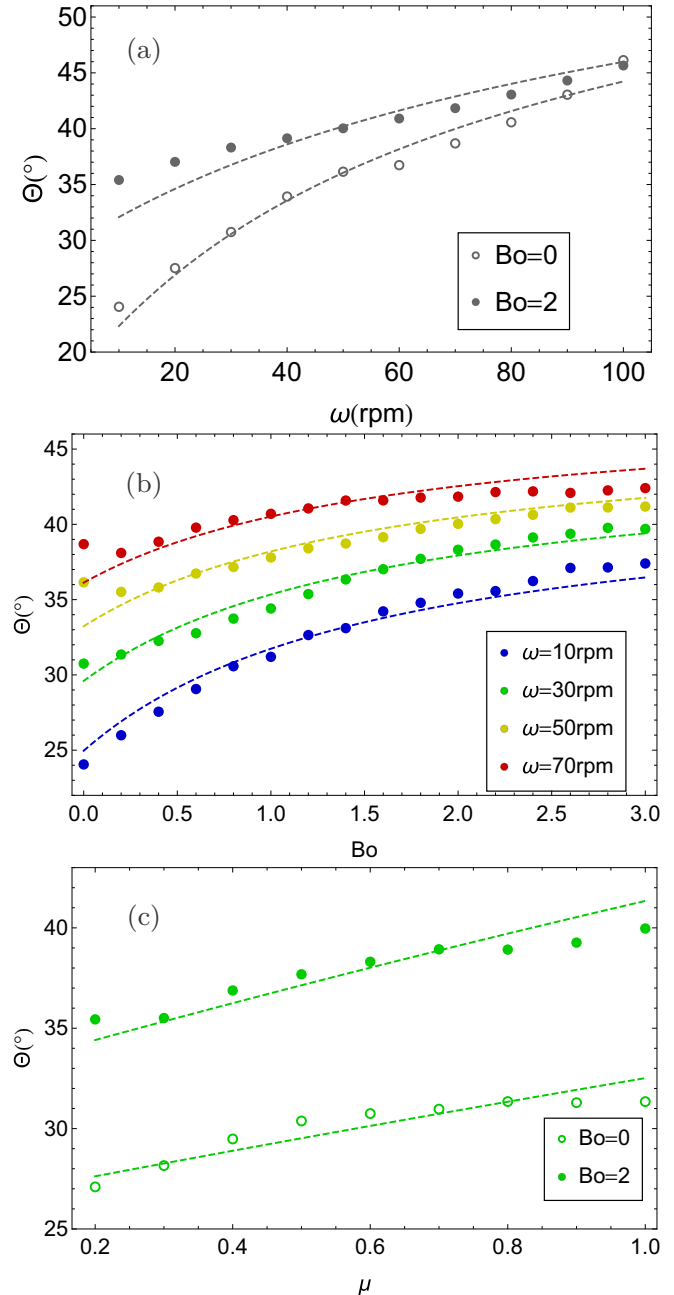


FIG. 4. Numerical measurement of the dynamic angle of repose as a function of (a) the rotation speed of the drum ω , (b) the cohesion given by Bo , and (c) the coefficient of friction μ . Dotted lines are the results of the theoretical model developed in Sec. III D.

remains identical if Bo is further increased. We also notice that if the surface is initially S shaped (i.e., at 50 and 70 rpm), the dynamic angle of repose slightly decreases at small Bo . We observe at the minimum of these curves that the S-shaped surface has completely disappeared.

The effect of the coefficient of friction in cohesive granular materials is also considered in this study and its effect on the dynamic angle of repose is shown in Fig. 4(c). We notice that the angle slowly increases with μ until the coefficient of friction reaches 0.6, and then remains roughly stable. As this coefficient of friction is also applied for contacts with

the drum, we assume that the smaller values of Θ at a low coefficient of friction are due to sliding on the drum. As μ increases, the grains progressively adhere on the surface of the drum and are thus carried further away. The dynamic angle of repose shall consequently increase.

With these measurements of the dynamic angle of repose and the velocity profile, we can conclude that our relatively simple model developed to reproduce the flow of cohesive granular material inside a rotating drum is accurate. Indeed, our numerical simulations present similar trends as previous experimental studies. Such qualitative agreement was also observed by Sunday *et al.* [42] and constitutes a validation of our approach. We also notice that the main feature of cohesive granular materials is the plug flow that helps us interpret the results we obtain in both measurements.

C. Surface fluctuations

In order to quantify the avalanches which occur when cohesive granular material flows inside the rotating drum, we measured the fluctuations of the surface. To measure the surface fluctuations, we determine at each time the grain-air interface of the granular bed. Then, we cumulate the data points over the whole simulation so that we obtain a cloud of points showing the surface layer in the rotating drum at all times. We divide the drum into J columns with a width of one grain diameter. Let y_i be the vertical position of point i in a certain column of the flowing layer composed of N points and \bar{y} the average height of the surface layer in that column. The standard deviation of the vertical position is then given by

$$\sigma = \sqrt{\frac{1}{N} \sum_{i=1}^N (y_i - \bar{y})^2}. \quad (7)$$

Once this calculation is done for each column, we plot the surface fluctuations as a function of the horizontal position x in the drum. We normalize the position x by the radius of the drum to obtain the measurement of $\sigma^*(\frac{x}{R})$ shown in Figs. 5(a)–5(c). If we compute the average over all the x positions, we obtain the mean surface fluctuations,

$$\langle \sigma^* \rangle = \frac{1}{J} \sum_{j=1}^J \sigma_j^*, \quad (8)$$

which are shown in Fig. 6. A similar measurement has been performed by Espiritu *et al.* [1], who looked instead at the surface roughness by measuring the length of the flowing surface.

We first observe in Fig. 5(a) that when Bo is set to 0 (purple points), the surface fluctuations remain roughly constant along the surface and equal to 2 grain radius. This means that the height of the flowing layer oscillates with an amplitude of the order of a grain size. This result tells us that the flow is continuous and that no plug flow could be observed which is coherent as the cohesion is set in this situation to 0. Once the Bo value is increased, we observe that the surface fluctuations increase proportionally. However, the growth rate seems to be more important when $x/R \sim -0.6$ and, to a lesser extent, when $x/R \sim 0.4$. If we refer to the illustrations shown in Table II to localize those fluctuations on the surface of the

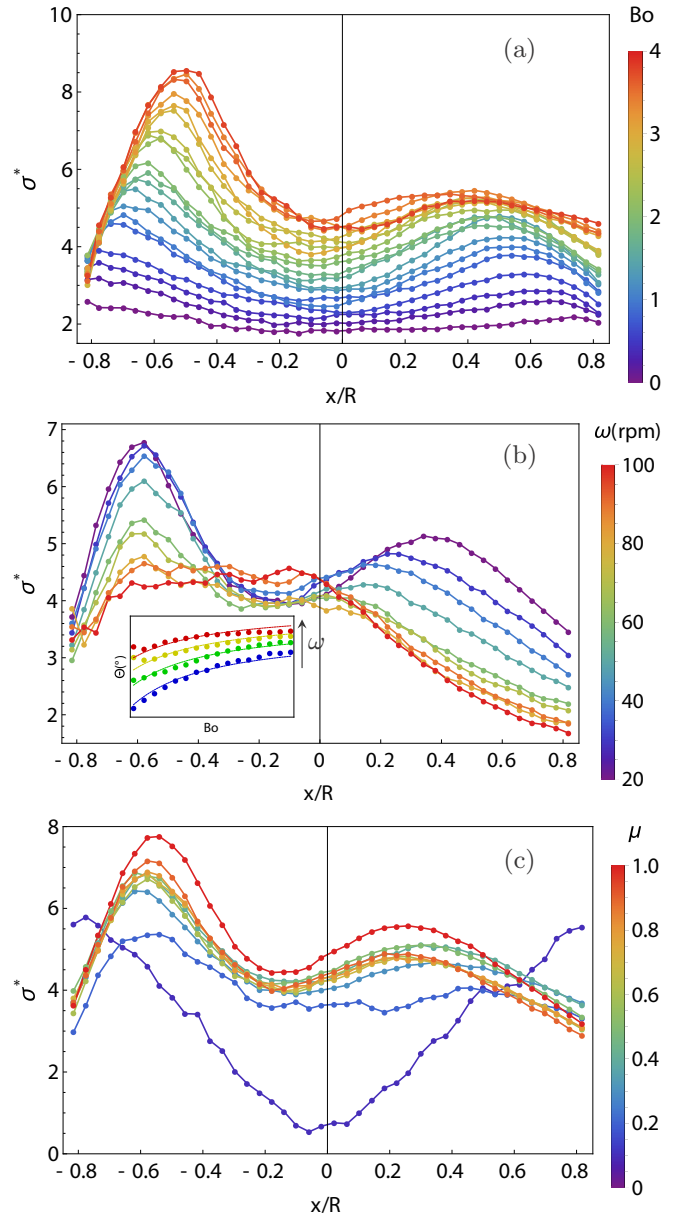


FIG. 5. Numerical measurements of flow fluctuations as a function of the position x in the laboratory reference frame and normalized by the drum radius R . The flow fluctuations σ have also been normalized by the grain radius $\sigma^* = \sigma/r$. (a) Effect of the rotation speed at $Bo = 2$ and $\mu = 0.6$. (b) Effect of the cohesion at $\omega = 30$ rpm and $\mu = 0.6$. Inset is a reproduction of Fig. 4(b). (c) Effect of the coefficient of friction at $Bo = 2$ and $\omega = 30$ rpm.

granular bed, they correspond, respectively, to the bottom of the surface on the left, where grains collide with the wall of the drum, and to the top on the right, where grains are fed to the surface. It can be interpreted as follows: firstly, the overall increase of the surface fluctuations tells us that plug flow is accentuated when cohesion is added. In other words, the size of the clusters flowing down on the surface increases with Bo . Second, the maximum at $x/R \sim 0.4$ is interpreted by the fact that when Bo is increased, the clusters are strongly bonded to the granular bed. A higher shear stress is thus required to detach the bigger clusters of grains. This shear

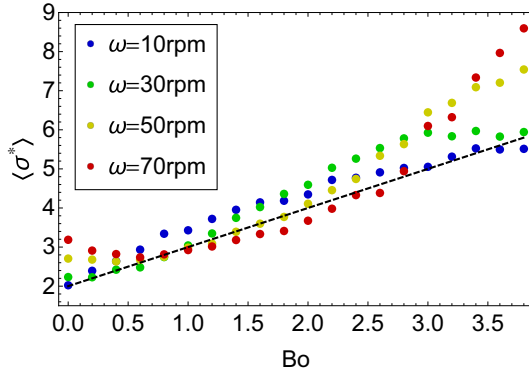


FIG. 6. Measurement of the mean surface flow fluctuations obtained from the results shown in Fig. 5 for $\mu = 0.6$. The black dashed line is a linear fit whose expression is given by $Bo + 2$.

stress comes from the weight of the cluster and increases with the angle of repose. As the cluster of grains is carried up by the drum, the shear stress, which is responsible for the creation of an avalanche, gradually increases up to the critical value to detach this cluster. The surface at this position consequently lowers. We also observe in Fig. 5(a) that surface fluctuations are relatively small near the center of the drum. This can be explained by the fact that once the avalanche has been triggered, the cluster of grains which flows down on the granular bed is still attracted by this granular bed. Due to friction between the flowing layer and the granular bed, a frictional shear stress exists between these two granular bodies. This shear stress tends to flatten the cluster of grains, and hence the lower surface fluctuations at the center of the drum. The sheared cluster of grains finally reaches the position $x/R \sim -0.6$ at the bottom of the granular bed where it hits the boundary of the drum. Depending on the rotation speed of the drum, it takes some time to transport this cluster of grains back up to the surface. As the rotation speed is set to a constant value but the size of the clusters flowing down is increased with the Bond number, we observe a second peak in surface fluctuations at the bottom of the granular bed as Bo increases.

That interpretation of cluster formation due to shear stress could also explain what we observe in Fig. 5(b). When ω increases, the surface fluctuations rapidly decrease. If we refer to the measurement of the dynamic angle of repose in the inset, we observe that the largest angles of repose are reached when the rotation speed is high. As the angle of repose is directly related to the shear stress responsible for plug flow, we observe that surface fluctuations around $x/R \sim 0.4$ decrease when ω is large. Also, when the rotation speed is large, we observe that the aggregates of grains at $x/R \sim -0.6$ are more rapidly evacuated as the fluctuations decrease when ω increases. We could thus assume that increasing the rotation speed of the drum reduces the intermittence of the flow.

Finally, we varied the coefficient of friction in a cohesive granular material and measured the surface fluctuations, as shown in Fig. 5(c). When the coefficient of friction is equal to 0.2, large fluctuations are observed at $x/R = \pm 0.8$ and nearly no fluctuations at the center of the drum. This tells us that the granular bed is actually in a stick-slip motion, which was impossible to observe in the previous average measurements

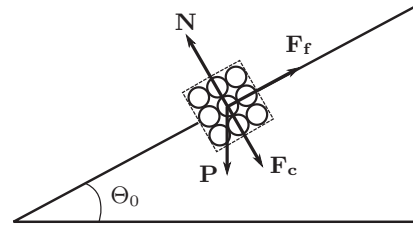


FIG. 7. Model for the forces on a cluster of grains flowing down on the granular bed represented by an inclined plane at an angle Θ_0 . F_c is the cohesive force exerted by the granular bed on the cluster, F_f is the friction force exerted by the granular bed on the cluster, N is the normal force exerted by the granular bed on the cluster, and P is the weight of the cluster.

of the angle of repose and the velocity profile. When μ is increased, the surface fluctuations rapidly collapse on one single curve, meaning that the coefficient of friction does not have a significant effect if it is high enough to avoid slipping.

In order to quantify the average size of the surface fluctuations, we measured the mean surface flow fluctuations $\langle \sigma^* \rangle$, as shown in Fig. 6. This measurement is defined by Eq. (8) and it provides an approximate size for the aggregates flowing at the surface of the granular bed as a function of Bo . If we compare the results obtained for different rotation speeds, we observe that the data seem to follow a linear law given by $Bo + 2$ (dashed line in Fig. 6). Thus, we obtain with this scaling that measuring the surface flow fluctuations gives a quantification of cohesion in the granular materials. It is interesting to note that the data deviate from this scaling at too high rotation speeds, meaning that this average size of plug flow is not as accurate in the cataracting regime, as discussed earlier with the velocity profiles.

D. Model for cohesive granular flow

A model has been derived by including cohesion in a theoretical development by Dury *et al.* [15]. By looking at the surface flows in a thin inclined layer or in the rotating drum, they obtained a relation for the dynamic angle of repose in noncohesive granular materials given by the following equation:

$$(y')^3 - (y')^2 \tan \Theta_0 + y' + c\omega(y^2 + x^2 - R^2) = \tan \Theta_0, \quad (9)$$

where $y' = \tan \Theta$, $\Theta_0 = \arctan \mu$ is the repose angle, x and y are position variables, and c is a parameter which is defined as granular viscosity. Since the repose angle is influenced by cohesion, a new expression of $\tan \Theta_0$ has to be found as the required repose angle for triggering an avalanche is influenced by cohesion, as discussed in Sec. III C. To determine the expression of $\tan \Theta_0$, we applied Newton's Second Law of Motion on a cluster of grains flowing at the surface. All the interactions between the cluster and the granular bed, both made of cohesive granular material, are represented in Fig. 7. One obtains (see the Appendix for detailed development)

$$\tan \Theta_0 = \left(1 + \frac{F_c}{P}\right)\mu. \quad (10)$$

In this equation, both F_c and P , the weight of the avalanche cluster, depend on the number of grains, N^* , that constitute

the cluster [see Eq. (A10) in the Appendix]. As mentioned before, the surface's height is fluctuating in average as $\langle \sigma^* \rangle \sim \text{Bo} + 2$. Considering that those fluctuations are due to plug flow, we can assume that this relation is directly related to the size of the clusters flowing at the surface. We obtain that clusters are made of $N^* = (\text{Bo}/2 + 1)^2$ grains. Based on that approximation, we find an expression for the ratio F_c/P given by

$$\frac{F_c}{P} = \sqrt{\pi} \frac{\text{Bo}}{\text{Bo} + 2}. \quad (11)$$

The expression of $\tan \Theta_0$ now includes the strength of cohesion given by Bo . We can introduce this expression into the model of Dury *et al.* given by Eq. (9) and solve it to determine how the dynamic angle of repose evolves with respect to ω , μ , and Bo . The solution is given in the Appendix in Eq. (A9).

If we plot this function with our numerical results, we can see in Figs. 4(a)–4(c) that the model perfectly fits the data. This result confirms the hypotheses we have made: we can assume that the flow of cohesive granular materials is characterized by an intermittent plug flow. In this context, the mean surface fluctuations represent a relevant measurement as they provide a correct approximation of the plug flow's magnitude, which depends on the strength of cohesion.

IV. CONCLUSION

We show that a simple attraction model for cohesion is able to reproduce the characteristic features of cohesive granular flow in the rotating drum. By performing the measurements of velocity profiles and dynamic angle of repose, we show indeed that the model leads to plug flow and the apparition of a convex grain-air interface, which are the characteristics of cohesive granular flow. We propose a measurement of surface flow fluctuations to capture, in the most efficient way, the effect of cohesion on granular flow. This measurement provides information about the dynamics of cluster formation at the surface of the granular bed which are at the basis of avalanches and plug flow. We also show that there exists a linear relation between surface fluctuations and the strength of cohesion in the granular material. Based on that scaling, we generalize the model for noncohesive granular flow by Dury *et al.* [15] to include cohesion and we compare it to numerical measurements. We obtain excellent agreement between theory and numerical data.

Beyond the fundamental character of the present study, the results and the associated model give a stronger theoretical basis for the interpretation of measurements made with rotating drums to characterize powder flow in industries. In particular, a better interpretation of the cohesive index measured with a GranuDrum instrument [4] can be achieved. This work could also find an application in additive manufacturing (AM) processes, as powder flowability is a key parameter to reach the high-quality standards fixed by industries [43]. In a previous publication [44], we have shown that numerical simulations of cohesive granular materials in the rotating drum could help to estimate the flowability of the powders used for AM. Finally, powder flow is also a topic of interest in planetary science, as the observation of sand dunes on planets could be used to determine the microscopic properties of soils [45–47].

As a perspective, we will implement realistic attractive interaction such as electrostatic forces between the grains to compare it with that simplified interaction potential.

ACKNOWLEDGMENT

The authors thank their colleagues from GRASP laboratory for valuable discussions.

APPENDIX: DEVELOPMENT OF THE MODEL

The model of cohesive granular flow is based on the Dury *et al.* model given by Eq. (9), which gives the dynamic angle of repose at any position of the granular bed's surface. To take cohesion into account in this equation, we have to find a new expression for $\tan \Theta_0$ which includes the strength of cohesion.

Applying Newton's Second Law of Motion on the cluster of grains under the action of the forces represented in Fig. 7 yields, along the direction of the inclined plane,

$$F_f - P \sin \Theta_0 = 0, \quad (A1)$$

and along the perpendicular of the inclined plane,

$$N - P \cos \Theta_0 - F_c = 0. \quad (A2)$$

Using Coulomb's law of friction and injecting Eq. (A2) into Eq. (A1), one has

$$\mu(P \cos \Theta_0 + F_c) - P \sin \Theta_0 = 0. \quad (A3)$$

The solution of this equation according to μ is then

$$\mu = \frac{P \sin \Theta_0}{P \cos \Theta_0 + F_c}. \quad (A4)$$

Using trigonometry, this equation becomes

$$\mu = \frac{\tan \Theta_0}{1 + \frac{F_c}{P} \sqrt{1 + \tan^2 \Theta_0}}. \quad (A5)$$

As $\tan \Theta_0$ must be positive, the only solution to this equation is

$$\tan \Theta_0 = \mu \frac{1 + \frac{F_c}{P} \sqrt{1 + \mu^2 \left[1 - \left(\frac{F_c}{P}\right)^2\right]}}{1 - \left(\frac{F_c}{P}\right)^2 \mu^2}. \quad (A6)$$

If $\mu < 1$, then $\mu^2 \ll 1$, so we can neglect terms with μ^2 . It remains then

$$\tan \Theta_0 = \mu \left(1 + \frac{F_c}{P}\right). \quad (A7)$$

This new expression for $\tan \Theta_0$ including the cohesive force is then injected in Dury's theoretical model [15] given by

$$(y')^3 - (y')^2 \tan \Theta_0 + y' + c\omega(y^2 + x^2 - R^2) = \tan \Theta_0, \quad (A8)$$

where $y' = \tan \Theta$. This equation is solved numerically with respect to y' at the center of the drum where we measure the dynamic angle of repose (i.e., $x = 0$ and $y = 0$), using Wolfram MATHEMATICA [48]. We obtain the following

solution:

$$\tan \Theta = \frac{\mu}{3} \left(1 + \frac{F_c}{P} \right) - \frac{A}{3} \left(\frac{2}{B + \sqrt{4A^3 + B^2}} \right)^{1/3} + \frac{1}{3} \left(\frac{B + \sqrt{4A^3 + B^2}}{2} \right)^{1/3}, \quad (\text{A9})$$

where

$$A = 3 - \left(\mu + \frac{F_c}{P} \mu \right)^2, \\ B = 18\mu + 18 \frac{F_c}{P} \mu + 27cR^2\omega.$$

We still have to evaluate the intensity of the forces F_c and P that are exerted on the cluster of grains flowing at the surface. The weight of the cluster P is given by the sum of each grain's weight, i.e., N^*mg , where N^* is the number of grains in the cluster and m is the mass of one grain. Let us consider that the cluster of grains flowing at the surface has the shape of a square; we obtain that the characteristic length of the cluster is given by $\sqrt{N^*\pi r^2}$. This length corresponds to the length of contact between the cluster and the granular bed. The number of grains from the cluster in contact with

the granular bed is then given by $\frac{\sqrt{N^*\pi r^2}}{2r}$. Consequently, we obtain

$$F_c = \frac{\sqrt{N^*\pi r^2}}{2r} mgBo. \quad (\text{A10})$$

The ratio F_c/P in Eq. (A9) is thus given by

$$\frac{F_c}{P} = \frac{1}{2} \sqrt{\frac{\pi}{N^*}} Bo. \quad (\text{A11})$$

The number of grains forming the cluster is approximated via the measurement of the mean surface fluctuations represented in Fig. 6. Indeed, at equilibrium between inertial forces and cohesive forces, we obtain a scaling for the mean surface fluctuations given by $\langle \sigma^* \rangle = Bo + 2$, as shown by the dotted line in Fig. 6. As the surface oscillates with an amplitude equal to $Bo + 2$ grain radius, we can assume that aggregates flowing down roughly contain $N^* = (Bo/2 + 1)^2$ grains. Equation (A11) thus becomes

$$\frac{F_c}{P} = \sqrt{\pi} \frac{Bo}{Bo + 2}. \quad (\text{A12})$$

This relation is then injected in the parameters A and B of Eq. (A9) to obtain an extended model of the dynamic angle of repose which includes cohesion with the fitting parameter c .

-
- [1] E. Espiritu, A. Kumar, A. Nommeots-Nomm, J. Lerma, and M. Brochu, *Powder Technol.* **366**, 925 (2020).
- [2] B. Chávez Montes, J. Martínez-Alejo, H. Lozano-Perez, J. Gummy, D. Zemlyanov, and M. Carvajal, *Powder Technol.* **357**, 269 (2019).
- [3] S. C. Thakur, O. I. Imole, M. B. Wojtkowski, V. Magnanimo, E. C. Montes, M. Ramaioli, H. Ahmadian, and J. Y. Ooi, Characterization of cohesive powders for bulk handling and DEM modelling, in *III International Conference on Particle-based Methods – Fundamentals and Applications, PARTICLES 2013*, edited by M. Bischoff, E. Oñate, D. R. J. Owen, E. Ramm, and P. Wriggers (2013), pp. 1–12.
- [4] G. Lumay, F. Boschini, K. Traina, S. Bontempi, J.-C. Remy, R. Cloots, and N. Vandewalle, *Powder Technol.* **224**, 19 (2012).
- [5] G. MiDi, *Eur. Phys. J. E* **14**, 341 (2004).
- [6] Y. Fan, Y. Boukerkour, T. Blanc, P. Umbanhowar, J. Ottino, and R. Lueptow, *Phys. Rev. E* **86**, 051305 (2012).
- [7] D. Khakhar, J. McCarthy, T. Shinbrot, and J. Ottino, *Phys. Fluids* **9**, 31 (1997).
- [8] N. Jain, J. Ottino, and R. Lueptow, *Phys. Fluids* **14**, 572 (2002).
- [9] E. Alizadeh, O. Dubé, F. Bertrand, and J. Chaouki, *AIChE J.* **59**, 1894 (2013).
- [10] D. Bonamy, F. Daviaud, and L. Laurent, *Phys. Fluids* **14**, 1666 (2002).
- [11] S.-Y. Lim, J. Davidson, R. Forster, D. Parker, D. Scott, and J. Seville, *Powder Technol.* **138**, 25 (2003).
- [12] D. Parker, A. Dijkstra, T. Martin, and J. Seville, *Chem. Eng. Sci.* **52**, 2011 (1997).
- [13] M. Rasouli, O. Dubé, F. Bertrand, and J. Chaouki, *AIChE J.* **62**, 2622 (2016).
- [14] M. Nakagawa, S. Altobelli, A. Caprihan, E. Fukushima, and E.-K. Jeong, *Expt. Fluids* **16**, 54 (1993).
- [15] C. M. Dury, G. H. Ristow, J. L. Moss, and M. Nakagawa, *Phys. Rev. E* **57**, 4491 (1998).
- [16] J. Mellmann, *Powder Technol.* **118**, 251 (2001).
- [17] R. Yang, A. Yu, L. McElroy, and J. Bao, *Powder Technol.* **188**, 170 (2008).
- [18] H. Komossa, S. Wirtz, V. Scherer, F. Herz, and E. Specht, *Powder Technol.* **264**, 96 (2014).
- [19] O. Dubé, E. Alizadeh, J. Chaouki, and F. Bertrand, *Chem. Eng. Sci.* **101**, 486 (2013).
- [20] N. Gui, X. Yang, J. Tu, S. Jiang, and Z. Zhang, *Particuology* **39**, 1 (2018).
- [21] S. He, J. Gan, D. Pinson, and Z. Zhou, *Powder Technol.* **341**, 157 (2019).
- [22] D. Santos, M. Barrozo, C. Duarte, F. Weigler, and J. Mellmann, *Adv. Powder Tech.* **27**, 692 (2016).
- [23] A. Alexander, B. Chaudhuri, A. Faqih, F. Muzzio, C. Davies, and M. Tomassone, *Powder Technol.* **164**, 13 (2006).
- [24] A. Rescaglio, J. Schockmel, N. Vandewalle, and G. Lumay, Combined effect of moisture and electrostatic charges on powder flow, *EPJ Web Conf.* **140** 13009 (2017).
- [25] M. Wojtkowski, O. I. Imole, M. Ramaioli, E. Chávez Montes, and S. Luding, Behavior of cohesive powder in rotating drums, in *Powders and Grains 2013: Proceedings of the 7th International Conference on Micromechanics of Granular Media*, edited by A. Yu, K. Dong, R. Yang, and S. Luding, AIP Conf. Proc. No. 1542 (AIP, New York, 2013), p. 983.
- [26] R. Brewster, G. S. Grest, and A. J. Levine, *Phys. Rev. E* **79**, 011305 (2009).
- [27] P. Liu, R. Yang, and A. Yu, *Phys. Fluids* **23**, 013304 (2011).

- [28] N. Taberlet, P. Richard, and E. John Hinch, *Phys. Rev. E* **73**, 050301(R) (2006).
- [29] X. Liu, W. Ma, Q. Hou, Q. Zhang, B. Gong, and Y. Feng, *Powder Technol.* **339**, 497 (2018).
- [30] A. Jarray, V. Magnanimo, M. Ramaioli, and S. Luding, Scaling of wet granular flows in a rotating drum, *EPJ Web Conf.* **140**, 03078 (2017).
- [31] A. Forsyth, S. Hutton, and M. Rhodes, *Powder Technol.* **126**, 150 (2002).
- [32] S. Luding, *Granul. Matter* **10**, 235 (2008).
- [33] N. Pohlman, J. Ottino, and R. Lueptow, *Phys. Rev. E* **74**, 031305 (2006).
- [34] P. Chen, J. Ottino, and R. Lueptow, *Phys. Rev. E* **78**, 021303 (2008).
- [35] A. Orpe and D. Khakhar, *Phys. Rev. E* **64**, 031302 (2001).
- [36] L. Orozco, J.-Y. Delenne, P. Sornay, and F. Radjai, *Phys. Rev. E* **101**, 052904 (2020).
- [37] M. Renouf, D. Bonamy, F. Dubois, and P. Alart, *Phys. Fluids* **17**, 103303 (2005).
- [38] F. Radjai and F. Dubois, *Discrete-element Modeling of Granular Materials* (Wiley-Iste, London, 2011).
- [39] S. Luding, *Eur. J. Environ. Civ. Eng.* **12**, 785 (2008).
- [40] S. Longo and A. Lamberti, *Expt. Fluids* **32**, 313 (2002).
- [41] H. Norouzi, R. Zarghami, and N. Mostoufi, *Chem. Eng. Res. Des.* **102**, 12 (2015).
- [42] C. Sunday, N. Murdoch, S. Tardivel, S. Schwartz, and P. Michel, *MNRAS* **498**, 1062 (2020).
- [43] G. Yablokova, M. Speirs, J. Van Humbeeck, J.-P. Kruth, J. Schrooten, R. Cloots, F. Boschini, G. Lumay, and J. Luyten, *Powder Technol.* **283**, 199 (2015).
- [44] N. Preud'homme, A. Neveu, F. Francqui, E. Opsomer, N. Vandewalle, and G. Lumay, Simulating powder bed based additive manufacturing processes: from DEM calibration to experimental validation, in *14th World Congress on Computational Mechanics (WCCM)*, edited by F. Chinesta, R. Abgrall, O. Allix, and M. Kalinske (2021).
- [45] M. Telfer, J. Parteli, J. Radebaugh, R. Beyer, T. Bertrand, F. Forget, F. Nimmo, W. Grundy, J. Moore, S. Alan Stern *et al.*, *Science* **360**, 992 (2018).
- [46] M. Kleinhans, H. Markies, S. De Vet, A. In't Veld, and F. Postema, *J. Geophys. Res. Planets* **116**, E11004 (2011).
- [47] R. Lorenz, S. Wall, J. Radebaugh, G. Boubin, E. Reffet, M. Janssen, E. Stofan, R. Lopes, R. Kirk, C. Elachi *et al.*, *Science* **312**, 724 (2006).
- [48] Mathematica, Version 12.3.1 (W. R. Inc., Champaign, IL, 2021), <https://www.wolfram.com/mathematica>.